International Conference on Mathematics and Computational Methods Applied to Nuclear Science and Engineering (M&C 2011)
Rio de Janeiro, RJ, Brazil, May 8-12, 2011, on CD-ROM, Latin American Section (LAS) / American Nuclear Society (ANS)
ISBN 978-85-63688-00-2

Evaluation of Charged Particles Multi-Scattering Theories for Microdosimetry

Cintra, F.B.*; Massicano, F.; Yoriyaz, H.
Centro de Engenharia Nuclear- Instituto de Pesquisas Energéticas e Nucleares- USP
Av. Prof. Lineu Prestes 2242 05508-000 São Paulo, SP- Brazil
*e-mail: fbcintra@ipen.br

ABSTRACT

In this work we have evaluated the multi-scattering functions for angular deflection and energy loss of charged particles in water medium. The most common models used nowadays are the Landau with Blunck-Leisegang-Seltzer corrections to energy straggling and Goudsmit-Saunderson or Molière theory for angular change. The evaluation has been done using a representative class I Monte Carlo code: the MCNP5 Monte Carlo radiation transport code. Electron sources with energies from 2 keV to 100 keV have been considered uniformly distributed in micrometer dimension water spheres with masses from 10^{-11} g up to 10^{-3} g. It was demonstrated here that parameters like the number of substeps, the energy straggling models and the geometry used play a very important role in the simulation process with strong influence on the estimated current and dose values. The conclusion is that reliable results are limited to problems with a range of geometric dimensions which also depends on the source particles energy.

Key Words: Microdosimetry, Multi-Scattering Theories, Computational Simulation.

1. INTRODUCTION

The Monte Carlo simulation of electrical charge transport and its interaction through matter is still a challenging computational problem. In part the complexity of this problem is due to the Coulomb interactions that must be accounted for in both scattering and bremsstrahlung emission interactions. This increases the number of interactions in several orders of magnitude, compared to photons or neutrons, to achieve a considerable change in spatial and energetic spectrum of charged particle, even in high density medium[1]. In Monte Carlo method each aspect of the particle history since its origin until its absorption or escape is performed sampling the probability functions that carry all geometric and physical aspects of the problem which is being simulated. As a consequence the complexity of the transport algorithm directly influences the performance of the simulation. Therefore, several numerical approaches become necessary to turn the simulation feasible in a reasonable period of time.

Introducing a new artificial parameter, the pathlength, Berger suggested that a certain number of perturbative interactions can be grouped and treated as one single virtual interaction[1]. The particle state transitions between pathlengths are obtained by sampling functions derived from multi-scattering theories. The most largely used theory in main general transport radiation codes are the Landau-Blunck-Leisegang for energy straggling and Goudsmit-Saunderson or Molière for angular changes. These theories are well established for most of the problems at macroscopic level with pathlengths and energies required in problems simulated in codes like MCNP[2], GEANT4[3] and EGSnrc[4]. However, applying multi-scattering theories in microscopic scale or/and in energy ranges from some eV's to few keV's requires special attention from the user.

The aim of this work is to present the limitations and possible adjustments needed to utilize these theories in microdosimetry problems which are gaining ground in the scientific community pursuing better comprehension of radiation damage at cellular level [5,6,7,8].

2. MULTI-SCATTERING THEORIES

2.1. The Landau Straggling Energy Function

In opposition to the continuous slowing down approximation (CSDA), the Landau model assumes that in a defined pathlength, *s*, the particle degrades its energy according to a distribution (not continually). It relates an universal auxiliary parameter λ with the energy loss Δ as shown in Equation (1)[9]:

$$f_L(\Delta, s)d\Delta = \varphi_L(\lambda)d\lambda \tag{1}$$

The function $\varphi(\lambda)$ was tabulated by Börsch-Supan[10].

In this model it's supposed that Δ is small compared with the initial energy of the particle at the beginning of the pathlength. The relation between Δ and λ is:

$$\Delta = \xi\left\{\lambda + \ln\left[\frac{2\xi mc^2\beta^2}{(1-\beta^2)I^2}\right] - \beta^2 + 0.4228 - \delta\right\} \tag{2}$$

where:
I is the medium mean excitation energy;
δ is the density correction factor;
β is the particle velocity relative to light velocity, *c* and;
m is the particle mass.

The parameter ξ can be written as:

$$\xi = \frac{0.154 MeV}{\beta^2}\frac{Z}{A}s \tag{3}$$

where:
Z is the atomic number;
A is the mass number and;
s is the pathlength.

As the distribution function in Equation (1) diverges in the energy domain, it is truncated using the collision stopping power to match the mean energy loss $\overline{\Delta}$:

$$\overline{\Delta} = \int_{S_n}^{S_{n+1}} \Delta f_L(\Delta, s) d\Delta = \int_{s_n}^{s_{n+1}} \left(dT/dx\right)_c dx \tag{4}$$

The interval between S_n and S_{n+1} defines a step and its distance is defined as the pathlength. The condition showed in Equation (4) is achieved redefining λ as:

$$\lambda \equiv \frac{\Delta - \overline{\Delta}}{\xi} + \nu^- \tag{5}$$

The variable ν^- is defined as (just for electrons):

$$\nu^- = \ln(T/\xi) - 0.80907 + \frac{\tau^2/8 - (2\tau+1)\ln(2)}{(\tau+1)^2} \tag{6}$$

where:
T is the kinetic energy of the particle, and;
$\tau = T/mc^2$.

Blunck-Leisegang account for the electron excitation resonances when calculating the energy loss straggling[11]. That correction was obtained by a convolution with a Gaussian distribution given by:

$$f^*(s,\Delta) = \frac{1}{\sqrt{2\pi}}\frac{1}{\sigma}\int_{-\infty}^{+\infty} f_L(s,\Delta')\exp\left[-\frac{(\Delta - \overline{\Delta})^2}{2\sigma^2}\right]d\Delta' \tag{7}$$

The FWHM of this Gaussian distribution were corrected by Seltzer to improve the precision for short pathlengths, so that σ is defined as follow:

$$\sigma = \frac{(10eV\, Z^{4/3}\, \overline{\Delta})^{1/2}}{1+3\left[\frac{10\xi}{I}\left(1+\frac{\xi}{10I}\right)^{3}\right]^{-1/2}} \tag{8}$$

However Matthews *et al*[12] adjusted empirically the function $\varphi(\lambda)$ as a sum of four Gaussian distributions obtaining:

$$\varphi(\lambda, b^2) = \sum_{i=1}^{4} \frac{\nu_i g_i}{\sqrt{b^2 + g_i^2}} \exp\left[-\frac{(\lambda-\lambda_i)^2}{b^2+g_i^2}\right] \tag{9}$$

where:

$b^2 = 2x10^{-5} Z^{4/3} Sp_{col} s/\xi^2$.
Sp_{col} is the collisional stopping power.

The constants ν_i, g_i and λ_i were calculated by Mukoyama and Watanabe[13]. These parameters are tabulated in Table I.

TABLE I. Parameters adjusted by Mukoyama and Watanabe[13] for all Gaussian distributions in Equation (9).

Adjusted	**index**			
Parameter	**1**	**2**	**3**	**4**
ν	0.124	0.0897	0.0443	0.024
g	1.16	1.38	2.26	7.34
λ	-0.712	0.781	2.639	4.386

2.2 The Molière Angular Deflection Function

The Molière angular deflection model provides the deflection angle by all elastic collisions (the main component responsible for changes in direction) within the pathlength, *s*, including sporadic catastrophic deflections. This model is limited by several conditions as listed below:

- Indistinguishable electrons and positrons;
- Small angle approximation ($\sin(x) \approx x$), used up to 30~40 degrees;
- Pathlength must include at least 20 collisions;
- The integrated energy loss in the whole pathlength must be negligible compared to the kinetic energy of the particle ($\Delta << T$).

The scattering angle is obtained in terms of a reduced variable ϑ .

$$\vartheta = \theta / \chi_c \sqrt{B} \tag{10}$$

where:

$$\chi_c = 0.6009 \frac{Z^2}{A} \left[\frac{\tau + 1}{\tau(\tau + 2)} \right]^2 s \tag{11}$$

and B is obtained solving the transcendental equation:

$$B - \ln(B) = \ln(\chi_c^2 / 1.167 \chi_a^2) \tag{12}$$

The variable χ_a^2 is given by Equation (13):

$$\chi_a^2 = \frac{6.8x10^{-5} Z^{2/3}}{\tau(\tau + 2)} \left[1.13 + 3.76 \left(\frac{Z}{137\beta} \right)^2 \right] \tag{13}$$

The angular distribution is related to the reduced angle as:

$$F_{Mol}(\theta, s)\theta d\theta = \vartheta d\vartheta \left[2e^{-\vartheta^2} + \frac{1}{B} f^{(1)}(\vartheta) + \frac{1}{B^2} f^{(2)}(\vartheta) + ... \right] \tag{14}$$

The terms in the expansion of Equation (14) are given by:

$$f^{(n)}(\vartheta) = \frac{1}{n!} \int_0^\infty u du \, J_0(u\vartheta) e^{-u^2/4} \left(\frac{u^2}{4} \ln \frac{u^2}{4} \right)^2 \tag{15}$$

where:

J_0 is the zero order Bessel function.

2.3 The Goudsmit-Saunderson Angular Deflection Function

The Goudsmit-Saunderson (G-S) model has a scattering angle distribution that can be expressed in a Legendre series. The main advantage of this function is that it is not based on small angle approximation. Therefore, it presents better results in wider scenarios when compared to the Molière model. The disadvantage is the relative higher difficulty to calculate the terms of the Legendre series and shorter pathlength implies poorer series convergence.

The G-S Probability density function is given by:

$$F_{GS}(\theta,s) = e^{-\mu s}\delta(\cos\theta - 1) + \mu s\, e^{-\mu s}\,\frac{2\pi}{\mu}\,\frac{N_a}{A}\,\sigma(\theta) + \sum_{l=0}^{\infty}(l+1/2)\left[e^{-sG_l} - e^{-\mu s}(1+\mu s - sG_l)\right]P_l(\cos\theta) \tag{16}$$

The variable s and θ are respectively the pathlength and the deflection angle. δ is the Dirac function, N_a is the Avogadro number A is the mass number of the medium, μ and G_l are showed in Equation (17) and Equation (18).

$$G_l = 2\pi\frac{N_a}{A}\int_0^{\pi}\left[1 - P_l(\cos\theta)\right]\sigma(\theta)\sin(\theta)d\theta \tag{17}$$

$$\mu = \frac{N_a}{A}\sigma_s = 2\pi\frac{N_a}{A}\int_0^{\pi}\sigma(\theta)\sin\theta\, d\theta \tag{18}$$

σ_s is the Møller scattering cross section.

3. MAIN SIMULATION PARAMETERS

General radiation transport codes can be divided in two main classes when simulating charged particles transport: class I and II. Class I codes utilize only the condensed history transport mode with the multi-scattering theories. There are generally one model to simulate the energy straggling and another to angular deflection. Two examples of these codes are MCNP and ETRAN. Class II codes are capable of segregate the particle collision in "soft" and "hard" from a preselected energy loss threshold. Hard collisions receive all the formalism of event by event simulation. On the other hand, soft collisions histories are condensed in a single history as in class I and it utilizes the multi-scattering theories for angular deflection, hence the name "mixed algorithm". Two examples of class II codes are PENELOPE and GEANT. In this sense, practically all general codes use some kind of condensed mode to streamline the simulation. Although Class II codes give more freedom and versatility to users to model their problems still many major codes stay exclusively in Class I transport mode.

Besides the pathlength some class I codes utilize a second parameter to improve the sampling process. This additional parameter was introduced into the algorithm in an attempt to reduce systematic errors generated by geometric surfaces in complex problems and especially in interfaces with different materials. They are called substeps and are obtained subdividing the pathlengths in a number of smaller steps. The energy straggling is sampled only once in a step (usually in the beginning of the step), then the correspondent energy loss is equally divided and assigned to each substep. On the other hand, the angular deflection is sampled at the substep level, taking advantage of the fact that the G-S function changes very slowly in a logarithmically spaced step allowing using the same function throughout all substeps.

4. METHOD

The main simulation tool used in this work that employ multi-scattering theories was the MCNP version 5. This code was developed at Los Alamos National Laboratory in the middle 50's. It was firstly used to modeling nuclear reactors and lately in dosimetry problems when electron transport package was included. It is a class I code, therefore it can simulate the charged particle transport only in condensed history mode. The step chosen to brief the particle history is the same form as the ETRAN code (8.3 % in energy loss at each step).

The energy loss is sampled using the Landau with Blunck-Leisegang probability density function (p.d.f.) and the deflection angle is sampled using the G-S p.d.f.. The atomic model used is the Thomas-Fermi, the cross sections are obtained with the Rutherford classical cross sections corrected to include relativistic and screening effects to energies until 0.256 MeV. Above this threshold the PWM (Partial Wave Method) is employed. The code can simulate the coupled transport of electrons and photons with energies between 1 keV up to 100 MeV.

In this work we have estimated the required number of substeps as a function of geometry sizes at microscopic level. The Landau energy straggling function with Blunck-Leisegang modification, called here as LBL model, has been also analyzed at microscopic dimensions. For this purpose, water spheres with masses ranging from 10^{-11}g up to 10^{-3}g immersed in water medium have been simulated and the energy deposition have been evaluated. It was imposed the condition of at least 10 *subteps* within the cell to assuring a precise trajectory[2]. This calculus was considered as if the monoenergetic electron source was pointwise and with initial energies from 2 keV up to 100 keV and located at the center of the spheres. The influence of steps corresponding to nearly 8.3% energy loss in the LBL distribution has been evaluated. The pathlength and the "10 substep rule" were chosen in order to preserve the validity of all multi-scattering theories used here specially the G-S model that needs at least ten samples in the interest medium to achieve a precise trajectory simulation[2].

After highlight the effects of the substep numbers in the simulation we have studied the influence of the number of geometric surfaces in the angle sampling. For this purpose, basically, we have modeled a 10^{-11}g water sphere involved by 9 concentric water spheres. Then we have tallied the angular distribution in each of 10 surfaces in a histogram with an angular bin interval of 10 degrees, as well as, the deposited energy in each of the cells for electrons with initial energy of 100 keV.

To add surfaces in MCNP we have used the geometric resource of repeated structures (voxels). It employed three different voxel sizes: 1%, 0.1% and 0.01% of CSDA range of source electrons. To store the electron incidence angle relative to normal vector in each surface it was used the F1 particle current tally divided in bins of 10 degrees (C card). To store the deposited energy in all volumes it was used the *F8 tally in all voxels within each cell.

5. RESULTS AND DISCUSSION

Table II shows the minimum number of substeps calculated imposing the condition that it is necessary at least 10 angular deflection samples inside the spheres in each case considered. The values were rounded to nearest integer. This division assured that the electron will in average has 10 substeps in the micrometric site.

Table II. Minimum number of substeps for each combination of energy and sphere radius. Numbers are rounded so zero means no substep needed.

Mass	Radius	Initial Energy (keV)											
(g)	(μm)	2	3	4	6	8	10	20	30	40	60	80	100
1E-11	1.34	0	0	1	1	2	3	10	21	32	68	106	163
3E-11	1.93	0	0	0	1	1	2	7	14	22	47	74	113
7E-11	2.56	0	0	0	1	1	1	5	11	17	36	55	85
1E-10	2.88	0	0	0	1	1	1	4	10	15	32	49	76
3E-10	4.15	0	0	0	0	1	1	3	7	10	22	34	52
7E-10	5.51	0	0	0	0	0	1	2	5	8	17	26	39
1E-09	6.20	0	0	0	0	0	1	2	4	7	15	23	35
1E-08	13.37	0	0	0	0	0	0	1	2	3	7	11	16
1E-07	28.79	0	0	0	0	0	0	0	1	2	3	5	8
1E-06	62.04	0	0	0	0	0	0	0	0	1	1	2	4
1E-05	133.65	0	0	0	0	0	0	0	0	0	1	1	2
1E-04	287.94	0	0	0	0	0	0	0	0	0	0	0	1
1E-03	620.35	0	0	0	0	0	0	0	0	0	0	0	0

It can be noted in all data presented that if the energy is constant the reduction of the sphere radius implies an increasing in the number of substeps. This is the consequence of the reduction of the space available for the step, so that, particles crossing tight spaces will employ more simulation time due to the higher number of substeps; this is the price that is necessary to maintain the correct trajectory of particle, mainly when studying deflection beams throughout thin foils.

For energies below 6 keV there is no need to divide the step even for the smallest sphere. But, at higher energies this changes in condition implies in larger sphere radius to be able to disregard the substeps. Other relevant information that can be observed is that the relationship between the simulation CPU time required for simulation and the number of substeps considered in a problem. For instance, a simulation using 200 substeps increases five times the CPU time compared to the same problem using 3 substeps. The worst case is the combination of high initial energy source in small spheres.

Figure 1 present the relationship between the sphere radius and the CSDA range for energies from 10 keV up to 100 keV. If the lateral displacement is disregarded one can infer in which cases the influence in the trajectory are more relevant. Particles with energy enough to cross

many surfaces are specially affected by any systematic error in deflected angle. Schaart *et al*[14] points other problem; in G-S model the maximum deflection angle was reduced when the presence of a surface interrupted the substep. This effect is sharper when this interruption happens in the beginning of the substep and as already observed by Schaart this lead to a underestimation of the high scattering angles.

After the Seltzer correction for $\xi / I < 10$ [15] the energy straggling distribution increased its precision for small pathlengths, so that, the use of the LBL model can be used without restriction, except when the condensed method seems useless (few collisions per history).

The importance of the empirically corrected FWHM by Seltzer (Equation (8)) in microdosimetry is obvious in Figure 2. The desirable substep number that could be used for the couple "initial energy - sphere radius" is below the m_max curve and above each curve in Figure 2. Values above the curve m_max imply an error greater than 3% in Landau p.d.f and generally it´s considered as unacceptable (see Equation (8)) [15]. Therefore without the correction term inserted into the denominator of Equation 8 practically no condition could be satisfied for the use of the Landau model. Every pathlength would be too small and the error in the energy loss would be unacceptable.

Figure 3 shows the differences between the Landau distribution with and without the terms related to the electron resonances inserted by Blunck-Lesisegang plus the Seltzer broad for small pathlengths to typical ETRAN pathlengths for several initial energies (8.3 % energy loss). It's possible to see that the lower the ratio ξ / I the greater the difference between the model with and without the corrections. This indicates that in this circumstance the electron resonance effect is even more important for the charged particle energy straggling and thus for the energy deposition along the track.

The strain in G-S p.d.f. is showed in Figure 4 when the deflecting angle is. Each surface is represented by its own histogram. Figure 4 shows the normalized angular distribution tallied with the F1 particle current tally card divided in bins of 10 degrees for three situations as follow: (a) the problem modeled without any voxel; (b) represent the geometry filled with voxel sizes of 0.1% of the CSDA range relative to source electrons; (c) represent the geometry filled with voxel sizes of 0.01% of the CSDA range relative to source electrons. It can be seen that for more distant layers from the source the greater will be the increase in frequency for bins corresponding to low angles. So it´s observed that electrons with same energy can be more penetrating if the user only changes the number of surfaces that cross the particle path. Although the physical problem modeled was basically the same, the presence of more or less number of surfaces introduced biased changes in the results. This behavior was already observed in other works [14,16,17].

Figure 5 shows the average angle calculated from the normalized frequencies showed in Figure 4 in each surface (1 until 10). The cases plotted here are only relatives to Figure 4a and 4c. The high relative uncertainties (same order of the average) are explained by the large width of the bins used (10 degrees). But this was necessary to achieve a reasonable simulation time. If one wants reduce these uncertainties then it´s necessary to reduce the bins to maybe 1 degree width.

The biased trajectory observed in electrons along the successive surfaces reflects in the energy deposition. Figure 6 shows that as electrons become more penetrating so they deposited less energy in all layers (cells) therefore carrying energy to longer distances from the source.

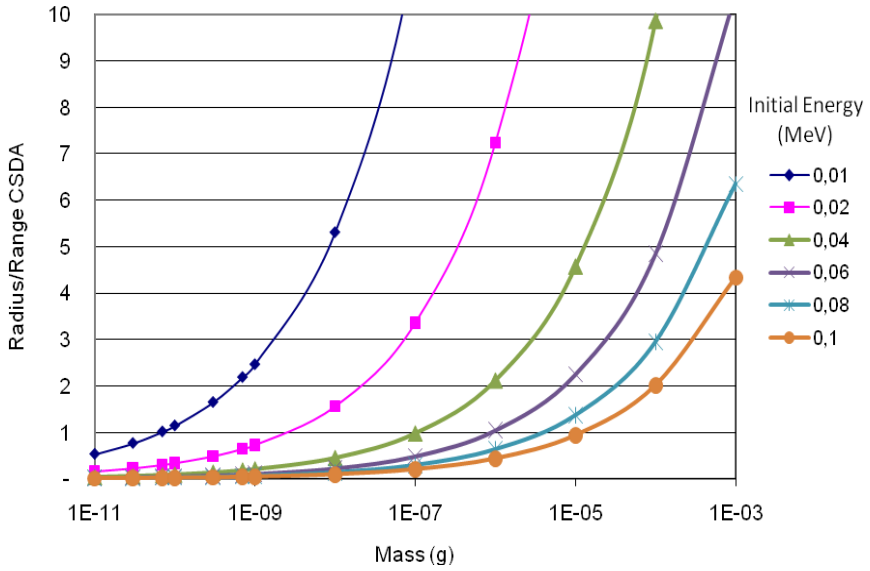

Figure 1. The sphere radius related to continuous slowing down approximation range. Ratios smaller than one means more crossing surfaces interrupting the charged particle step, considering the 8.3 % logarithmic step decrease.

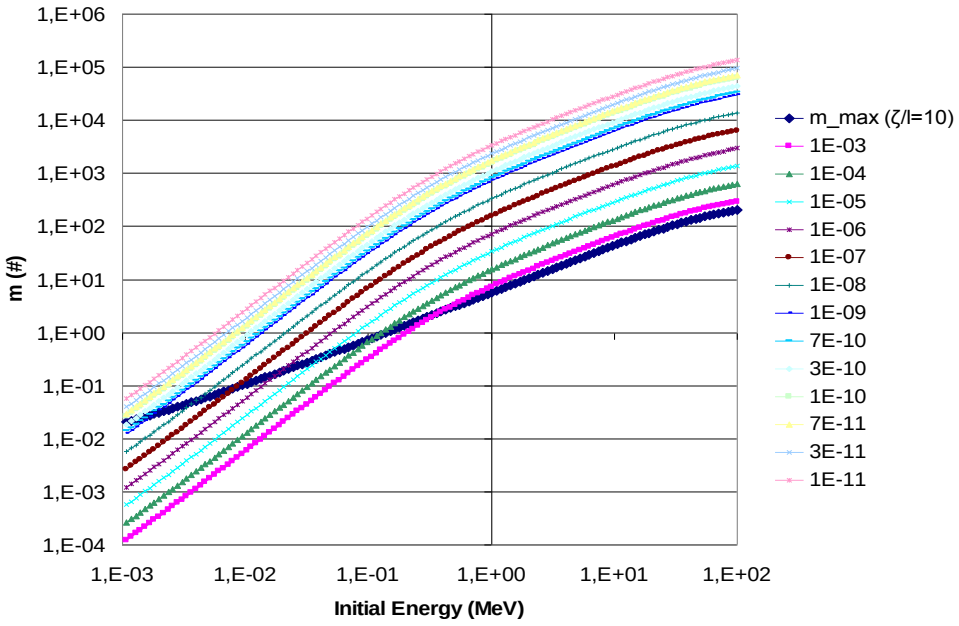

Figure 2. The validity range for substep number without the Seltzer correction for small pathlengths. Values above the "m_max" curve implies error higher than 3 % in Landau

p.d.f.. Each curve is related to a sphere mass, except by the m_max curve that shows the number of substep for $\xi / I = 10$.

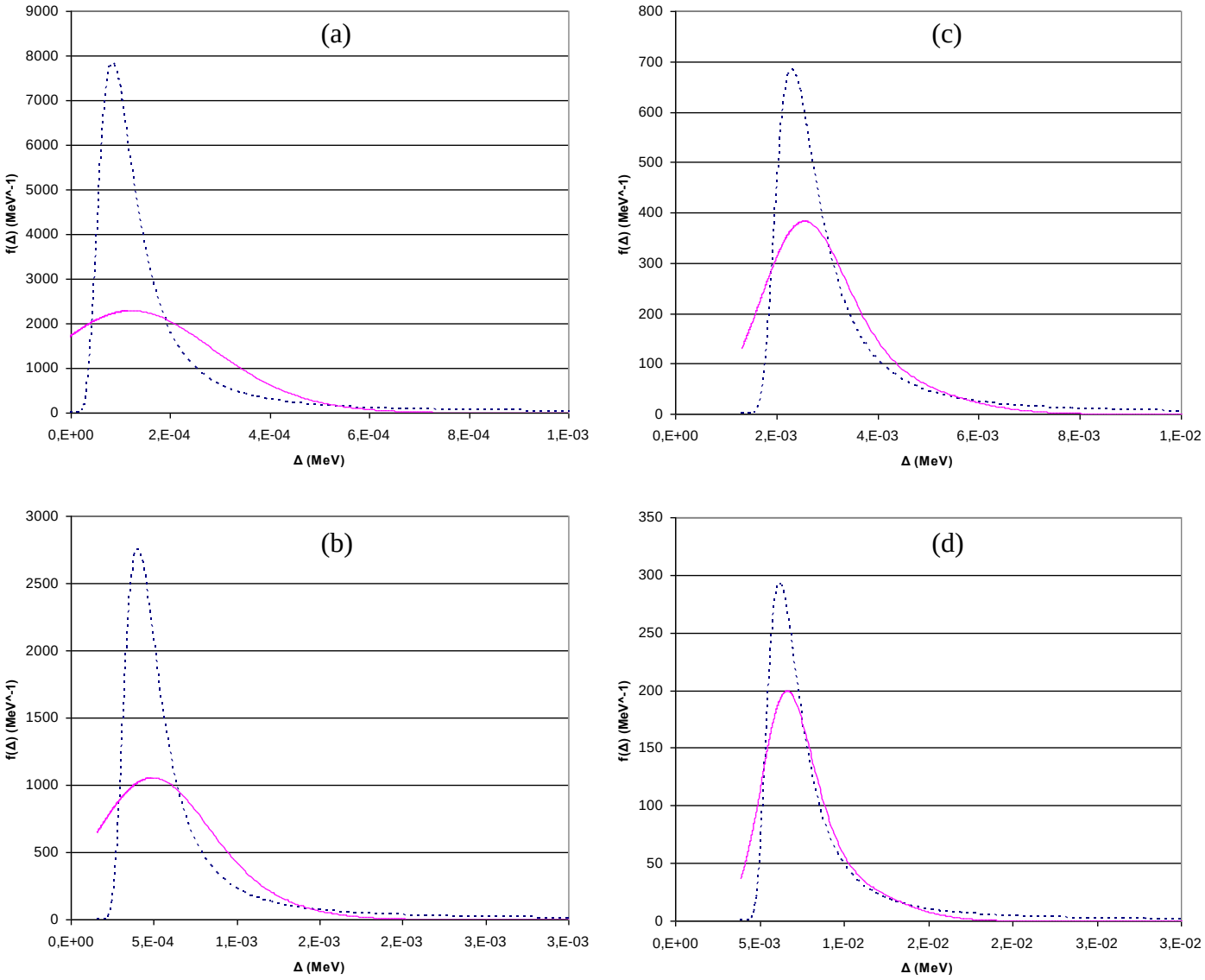

Figure 3. Differences between straggling functions of Landau (full line) and LBL plus the Seltzer broadening (dotted line) for (a) 2 keV, 0.021µm, $\xi / I = 0.31$; (b) 8 keV, 0.23 µm, $\xi / I = 0.87$; (c) 40 keV, 4.33 µm, $\xi / I = 3.5$; (d) 100 keV, 21.77 µm, $\xi / I = 8.2$.

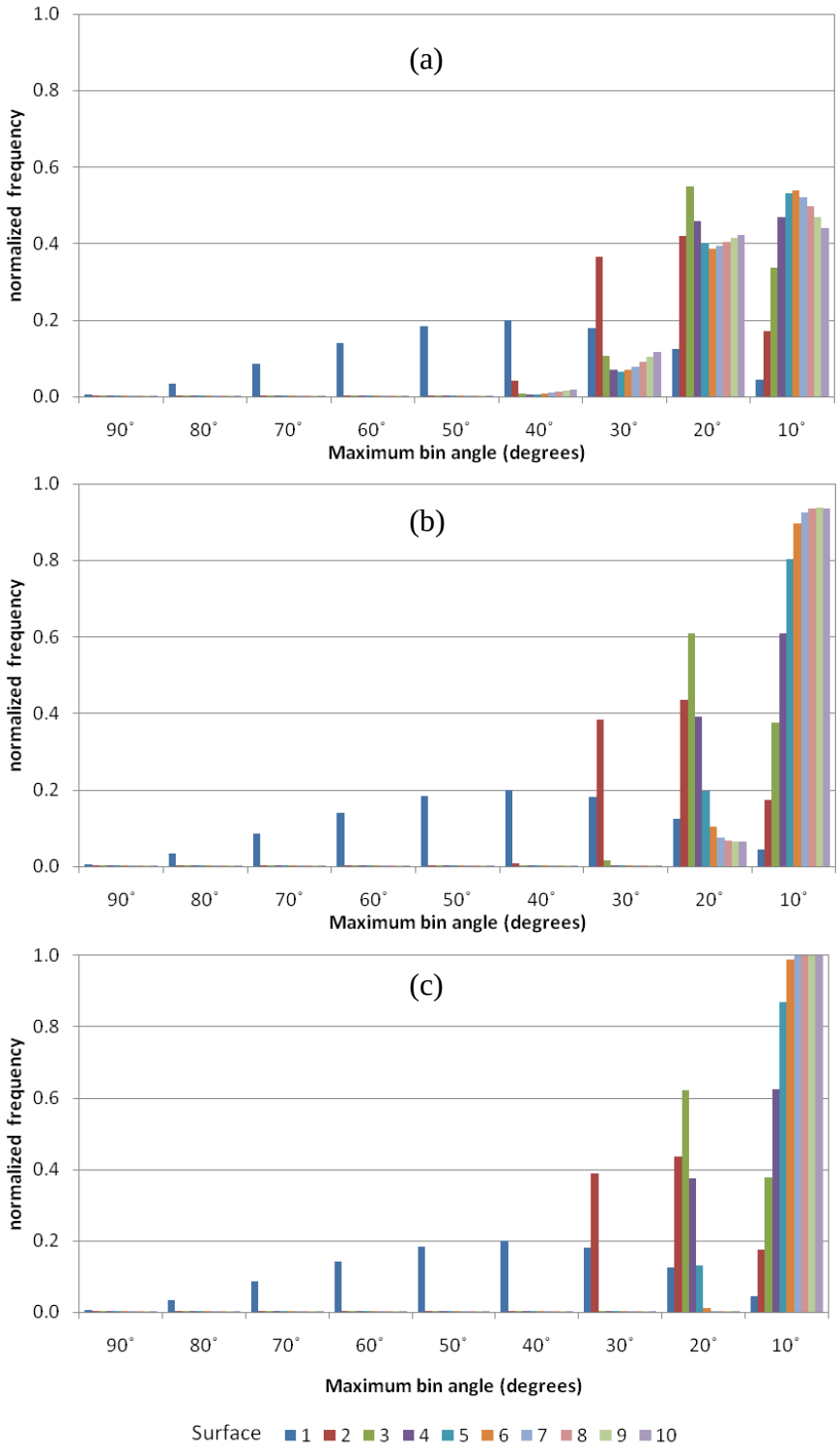

Figure 4. Normalized angular distribution for three different situations: (a) the problem modeled without any voxel; (b) represent the geometry filled with voxels which size is 0.1% of the CSDA range relative to source electrons; (c) represent the geometry filled with voxels which size is 0.01% of the CSDA range relative to source electrons (100 keV).

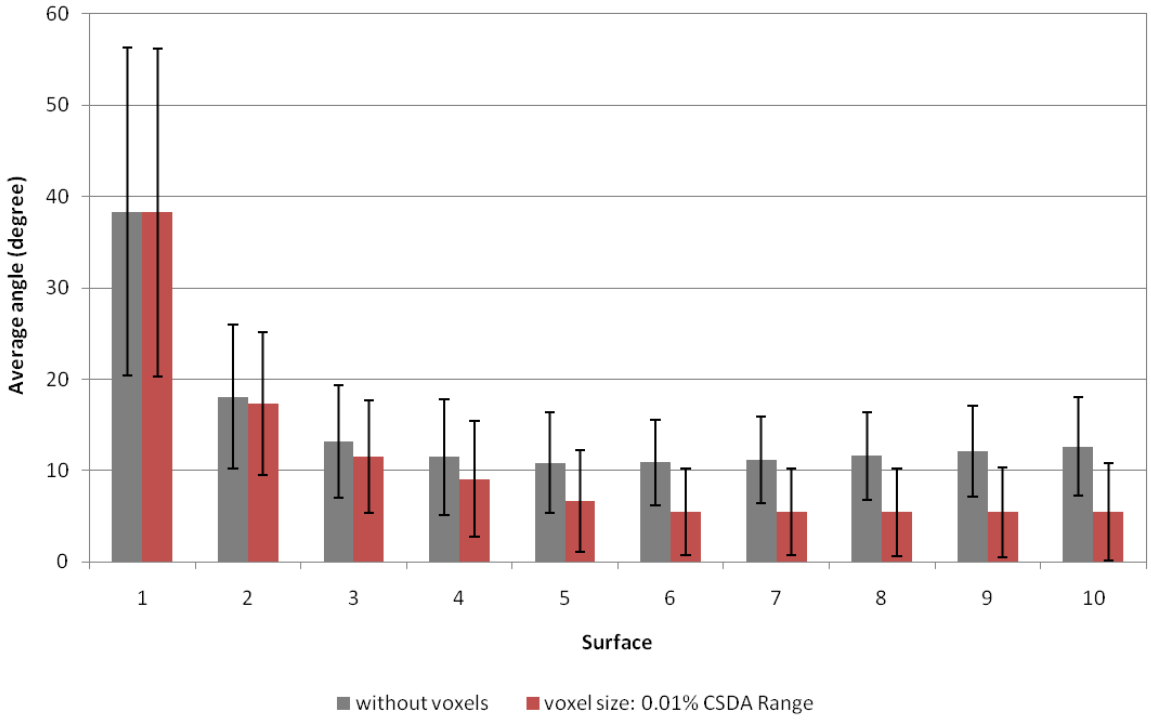

Figure 5. Average angle calculated from the normalized frequencies in Figure 4a and 4c for each surface for a 100 keV electron source.

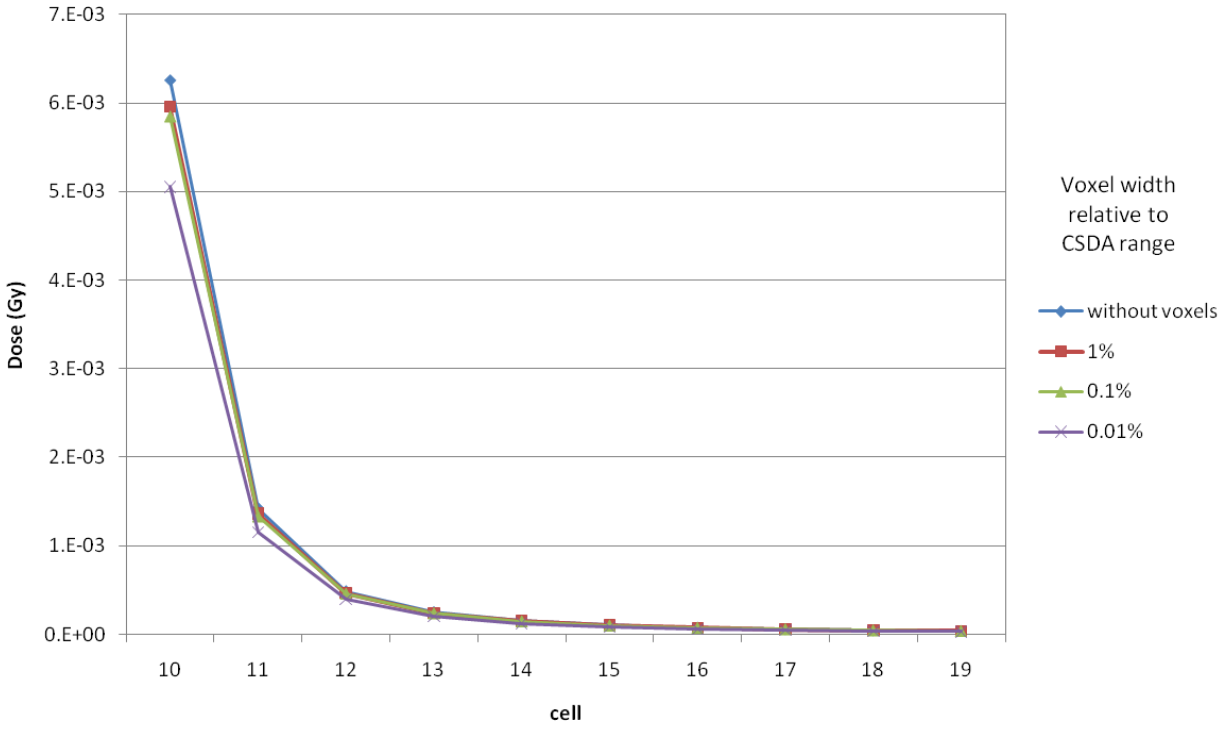

Figure 6. Dose deposition in each layer (cell) for a 100 keV electron source.

6. CONCLUSIONS

In this work it was evaluated the multi-scattering theories used by major transport codes as MCNP, GEANT and EGS applied in a micrometric pathlengths and low energy electrons (2 keV – 100 keV) in water medium. These models are used to make the transport of charged particles more efficient due to the long range Coulomb force. It was evaluated the best simulation parameters when the Landau+Blunck-Leisegang plus the Seltzer broadening and the Goudsmit-Saunderson are combined. The main parameter that the user can change is the substep number where the angular deflection is sampled and secondary particles are generated. This was done to simulate more accurately the trajectory of the charged particle and avoid systematic errors in energy loss when crossing an interface between two different materials. The recommended substep numbers required for each scenario of initial energy and typical volume where the particle is being transported have been quantified.

This work also showed the relevance of the Seltzer broadening for the spatial and energetic scale approaching. The Landau model was only suitable to these situations because the insertion all corrections. The ratio ξ / I plays the main role when these functions are evaluated, so that, the higher the ratio the lower the influence of the simulation refinements.

Finally it was evaluated the influences of crossing surfaces in electron trajectory specifically in how this effect changes both the average incident angle in a specific surface, as well as, the energy that this electrons can carry for larger distances. Although all cases represent the same physical problem the results change according to the way the geometry are designed. The uncertainties achieved here do not allow quantitative values but indicates a well known behavior in G-S model when the step is interrupted. In general, the increasing number of crossing surfaces affects the average angle relative to normal surface direction.

7. ACKNOWLEDGMENTS

The Authors thank the Comissão Nacional de Energia Nuclear (CNEN) for partial economic support.

8. REFERENCES

1. Berger, M. J. Monte Carlo Calculations of the Penetration and Diffusion of Fast Charged Particles, *Methods in Computational Physics*, Academic Press NY, v.1, pp. 135-215, 1963.

2. X-5 Monte Carlo Team. MCNP: A General Monte Carlo N-Particle Transport Code, version 5. Report LA-CP-03-0245, *Los Alamos National Laboratory*, Los Alamos, New Mexico, 2003.

3. Agostinelli, S. Geant4 – A Simulation Toolkit. *Nuclear Instruments and Methods in Physics Research A*, v. 503, pp. 250-303, 2003.

4. Kawrakow, I.; Rogers, D.W.O. The EGSnrc Code System: Monte Carlo Simulation of Electron and Photon Transport, Institute for National Measurements Standards, pp. 50, Avaiable at <http://www.irs.inms.nrc.ca/EGSnrc/EGSnrc.html>, accessed on September 2010.

5. Cox, R.; Thacker, J.; Goodhead, D.T. Inactivation and Mutation of Cultured Mammaliam Cells by Aluminum Characteristic Ultrasoft X-Rays, *International Journal of Radiation Biology*, n. 31, pp. 561-576, 1977.

6. Goodhead, D.T.; Thacker, J.; Cox, J. Effectiveness of 0.3 keV Carbon Ultrasoft X-Rays for the Inactivation and Mutation of Cultured Mammalian Cells, *International Journal of Radiation Biology*, n. 36, pp. 101-114 ,1979.

7. Raju, M.R. et al. Radiobiology of Ultrasoft X-Rays. *Annual Meeting of the Radiation Research Society*, ed. 32, pp. 99,1984.

8. Thacker, J.; Wilkinson, R.E.; Goodhead, D.T. The Induction of Chromosome Exchange Aberrations by Carbon Ultrasoft X-Rays in V79 Hamster Cells. *International Journal of Radiation Biology*, n. 49, pp. 645-656, 1986.

9. Seltzer, S.M. Electron-Photon Monte Carlo Calculations: The ETRAN Code, *Applied Radiation and Isotopes*, v. 42, pp. 917-941, 1991.

10. Börsch-Supan, W. On the Evaluation of the $\phi(\lambda) = \frac{1}{2\pi i}\int_{\sigma-ix}^{\sigma+ix} e^{u\ln(u)+\lambda u}\,du$ Function for Real Values of λ, *Journal of Research of the National Bureau of Standards B*, v. 65, n. 4, pp. 245-250, 1961.

11. Mejaddem, Y. *et al*. Calculations of Electron Energy Loss Straggling, *Nuclear Instruments and Methods in Physics Research B*, v. 173, pp. 397-410, 2001.

12. Matthews, J.L.; Findlay, D.J.S.; Owens, R.O. The Distribution of Electron-Energy Losses in Thin Absorbers, *Nuclear Instruments & Methods*, v. 180, n. 2-3, pp. 573-579, 1981.

13. Mukoyama, T.; Watanabe, Y. On The Energy Loss of Fast Electrons in Thin Absorbers, *Physics Letters A*, v. 64, n. 5, pp. 442-443, 1977.

14. Schaart, D. et al. A Comparison of MCNP4C Electron Transport with ITS 3.0 and Experiment at Energies Between 100 keV and 20 MeV: Influence of Voxel Size, Substeps and Energy Indexing Algorithm, *Physics in Medicine and Biology*, v. 7, pp. 1459-1484, 2002.

15. Berger, M. J.; Wang, R. Multiple-Scattering Angular Deflections and Energy-Loss Straggling, *Monte Carlo Transport of Electron and Photons*, Academic Press New York, cap. 2, pp. 21-56, 1988.

16. Hughes, H.G. Treating Electron Transport in MCNP, Report LA-UR-96-4583, *Los Alamos National Laboratory*, Los Alamos, New Mexico, 1996.

17. Yoriyaz, H. et al. Physical models, cross sections, and numerical approximations used in MCNP and GEANT4 Monte Carlo codes for photon and electron absorbed fraction calculation, *Medical Physics*, v. 36, Issue 11, pp.5198-5213, 2009.